Progress In Electromagnetics Research, PIER 104, 31–48, 2010

FEM ANALYSIS OF ANGULAR MISALIGNMENT FAULT IN SRM MAGNETOSTATIC CHARACTERISTICS

H. Torkaman

Young Researchers Club
I.A.U., South Tehran Branch
Tehran, Iran

E. Afjei

Department of Electrical Engineering
Shahid Beheshti University
Tehran, Iran

Abstract—This paper proposes magnetostatic analysis of Switched Reluctance Motor (SRM) under angular misalignment fault to evaluate the performance of the motor under different operating conditions. In this analysis three-dimensional finite element method (FEM) is used to simulate reliable and precise model by considering the complex motor magnetic geometry, end effects, axial fringing effects as well as nonlinear properties of the magnetic materials. The FE analysis is performed to obtain the static magnetic characteristics of SRM including flux density, flux linkages, terminal inductance and mutual inductance profile under different rotor positions for different varying degree of faults. Consequently, it presents assessing the features of mutual inductance in inactive phases to study the variations of diagnosis index. The results obtained present useful information regarding the detection of fault and its direction as well as the amount of angular misalignment fault in the motor. To the best knowledge of the authors, such an analysis has not been carried out previously.

1. INTRODUCTION

The magnetic characteristics analysis of a Switched Reluctance Motor in normal and abnormal conditions are important in performance prediction and verification of the motor [1–3]. The nonexistence of

Corresponding author: H. Torkaman (H_Torkaman@sbu.ac.ir).

permanent magnet in SRM reduces many hazards of the machine in comparison to permanent magnet machines, which makes it perfectly suitable for various applications [4]. However, the fault tolerance of the SRM is not absolute, and it must be studied with several qualifications [5]. Therefore, the fault analysis and diagnosis in the SR motor for operation with high efficiency has required particular consideration in decreasing vibration, noise, operating temperatures, wear on mechanical systems, and downtime due to breakage.

Eccentricity fault is one of the most frequent sources of failure in electric machines. Therefore, it is essential and unavoidable to analysis and diagnosis the eccentricity in order to achieve a suitable control for smooth running of the motor. Eccentricity exists in a motor when there is a non-uniform air gap between the stator and the rotor, may it be due to mechanical causes or to faults in the electric or magnetic system.

Eccentricity consists of three types, namely static, dynamic and mixed eccentricities. From the other point of view, rotor misalignment can be defined as a different type of eccentricity. This type of eccentricity is caused by axial uneven airgap along with "z" axis or stator length dissimilar to other eccentricity that occurs along with "x, y" axes or stator width. In other words, the air gap length is a function of the rotor angle and the position along the axial dimensions in misalignment. When this type of fault attends to angular and axial uneven airgap along with "z" axis, it can be named angular misalignment.

Misalignment increases unplanned machinery downtime resulting in higher maintenance costs and loss of power production. In addition, misaligned rotor can increase vibration levels and friction, which can significantly increases energy consumption and can cause premature bearing failures. This type of fault causes potentially high stresses in the couplings, shafts, bearings, and seals. Generally, angularly and axially rotor misplacement reduces the steady-state performance and the operating life.

In recent years, there has been widespread interest in the fault analysis in electrical machines. The effects of misalignment or angular misalignment fault has been addressed in other motors and applications such as [6–8], while this analysis has not been considered in depth analysis for application in SRM, and this paper is an attempt to achieve that purpose.

In the following some reviews of eccentricity evaluation in SRM are considered. In [9], two dimensional Finite Element (2D-FE) coupled with quasi Newton-Raphson method are used to analyze dynamic eccentricity. It declared that the field distribution and torque in faulty

motor can be less or more than healthy motor, which depend on the rotor position and the currents exciting of the stator phases. In [10], the static eccentricity in different types of stator winding is analyzed by coupled 2D-FE with external circuit.

In [11], different modes of vibration which are caused by eccentricity have been analyzed by 2D-FE, and has been shown that resonant frequencies go along with even modes of vibration.

Dynamic eccentricity utilizing transient 2D-FE has been done in [12]. They are shown that in 33% eccentricity, the Unbalanced Magnetic Pull (UMP) has increased from 0.02 up to 400 N. Consequently, fundamental and 7th component are dominant frequencies. In [13], a linear analytical model for SRM in order to use vibration as an index in eccentricity diagnosis is presented. In this model, the airgap is defined as a function of time and place. When 30% eccentricity happens, the torque of the shaft increases 5%. Fundamental component of Radial Force (RF) is dominant frequency with a magnitude10 times as much as healthy condition.

Dynamic response of the motor under static and dynamic eccentricities are studied by [14] using coupled 2D-FE in Matlab environment.

In [15], it has been shown that the torque increased only by 1.8–2.4% within occurrence of dynamic eccentricity. After processing nodal vibration caused by fault in [16] they introduced harmonic components of vibration as a diagnostic tool to study eccentricity. As well, it has shown that RF and torque were increased up to 100 N. and 5%, respectively, with the presence of 33% dynamic eccentricity.

In [17], the static and dynamic eccentricities in a SRM were investigated. The authors improved a magnetic equivalent circuit method for force prediction accurately and quickly. They showed that, the Unbalanced Magnetic Force (UMF) grows almost linearly with the increasing relative eccentricity. An analytical model for RF evaluation in [18], which is caused by eccentricity, presented and verified by FE. It shows that RF increased linearly by growing the static eccentricity. The value of the force depends on the rotor position and the phase current.

In the earlier works, the author has analyzed the SRM [19] and Switched Reluctance Generator (SRG) [3, 20, 21] under healthy mode utilizing 3D-FEM, then in [22] the static eccentricity in the same motor is assessed and the dynamic eccentricity is evaluated and presented in [2]. Afterward, the intervals for different modes of motor operation (normal and faulty) are calculated by a hybrid method in [1]. Consequently, the effect of angular rotor misalignment in SRM is taken into account, in this paper.

Some significant contribution of this paper distinguish it from previous researches: a) comprehensive angular misalignment fault analysis in SRM, b) implementation of the faulty and normal SRM model in three dimensional FEM taking into account the end effects and axial fringing fields in SRMs modeling, and c) a 360 degree rotation of the rotor is considered due to essence of this fault analysis.

This paper is structured as follows: In Section 2, the definition of angular misalignment in motor operation is presented. Section 3 deals with the SRM modeling and specifications of implemented motor. The finite element results of the motor profiles under angular misalignment fault and normal are obtained and debated in Section 4. Consequently, in Section 5, some concluding notes are presented.

2. PRINCIPLE OF ANGULAR MISALIGNED ROTOR IN A SR MOTOR

As mentioned before, misalignment fault or axial eccentricity appears when there is variation of the eccentricities along the axis of rotor. In addition, angular misalignment or angular and axial eccentricity occurs when there is variation of the eccentricities along the axis of rotor with rotational rotor movement. In this type of misplaced rotor fault the air gap length in cross of stator poles is time variant. As, in misalignment the rotor rotates around its axis that is parallel and tangent with rotational axis, however, in angular misalignment the axis of rotor is not parallel to the stator and rotational axes and, has different eccentricity in each section of the machine. In other words, in this case the rotational axis is parallel and tangent with stator axis, so are different from rotor axis. Fig. 1 shows the cross section of the rotor movement (for two positions) in inner stator space when the motor faced with angular misalignment. This case may caused by improper alignment of right and left bearing centers, centrifugal phenomena, oscillation of connected load to the shaft, shaft deflection due to thermal distortions or externally imposed misaligning moments.

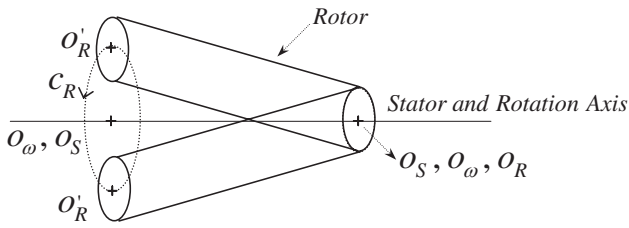

Figure 1. Rotational motion of the rotor in angular misalignment fault.

O_ω and O_s are the rotor rotation center and stator symmetry center. O_R, O'_R and C_R are the rotor center in right bearing, rotor center in left bearing and the rout of rotor rotation in one period with 360 degree rotation, respectively. In this type of fault that illustrated in Fig. 1; $O_R = O_\omega = O_s$ in right section of the motor and $O'_R \neq O_\omega = O_s$ in left section of the motor. Angular rotor misalignment monitoring index (ARMMI) is calculated to represent the angular misalignment degree or percentage of angular misalignment for each output data. The ARMMI is defined as the relative alignment condition;

$$\varepsilon_{AMis} = \left(\frac{\delta}{\beta}\right) \times 100(\%) \tag{1}$$

where ε_{AMis} is the percentage of angular misalignment fault between the stator and rotor axes, β is the maximum allowable unalignment before rubbing starts between the rotor and stator, and δ is the ratio of actual instantaneous unalignment or is the displacement of the rotor in the vertical direction to the excited stator poles in aligned position. Due to tolerance variation in manufacture and assembly, there is always an inherent asymmetry of the airgap between the stator and rotor axes; consequently, more than 10% misalignment is considered in this study. The relative misalignment of more than 50% is not considered here due to collision of the rotor pole with the stator pole.

3. FINITE ELEMENT MODELING OF SRM UNDER FAULTY AND HEALTHY OPERATIONS

Accurate and reliable modeling of the electrical systems is essential in performance prediction and verification of the systems [23–29]. The Finite Element Method can be one of the best choices for providing realistic and precise model [30, 31, 36–38]. Also, 3D-FEM has advantages over 2D in many applications modeling [32, 33], for example the skew effect, end ring effect and some other practical issues such as motor length are missed in two dimensional analyses. This method considers the geometric and magnetic of the motor to solve for the magnetic field distribution in and around the motor. Moreover, machine parameters such as flux density, flux linkage, coil inductance and torque can be achieved from resulted magnetic field.

The SRM modeling under normal and abnormal conditions is complicated in comparison with the ac or dc machines because of operating in nonlinear region. Therefore, in this study a three dimensional finite element [34] is being employed to assess the magnetic field distribution in and around the motor. In order to present the operation of the motor and to determine the motor parameters at

different positions of the rotor, the field solutions are obtained. There are two common methods for solving magnetic field problems one utilizes magnetic vector potential A and the other one employs electric vector potential T. The partial differential equation for the magnetic vector potential is given by;

$$-\frac{\partial}{\partial x}\left(\gamma\frac{\partial\bar{A}}{\partial x}\right)-\frac{\partial}{\partial y}\left(\gamma\frac{\partial\bar{A}}{\partial y}\right)-\frac{\partial}{\partial z}\left(\gamma\frac{\partial\bar{A}}{\partial z}\right)=J \tag{2}$$

where, J and A are the current density and magnetic vector potential.

In the variational method the solution to (2) is obtained by minimizing the following functional;

$$F(\bar{A})=\frac{1}{2}\iiint_{\alpha}\left[\gamma\left(\frac{\partial\bar{A}}{\partial x}\right)^{2}+\gamma\left(\frac{\partial\bar{A}}{\partial y}\right)^{2}+\gamma\left(\frac{\partial\bar{A}}{\partial z}\right)^{2}\right]d\alpha-\iiint_{\alpha}J\bar{A}d\alpha \tag{3}$$

where, α is the problem region of integration. The field analysis has been performed using a MagNet package which is based on the variational energy minimization technique to solve for the electric vector potential. In this method, electric vector potential known as $T-\Omega$ formulation in there T defined by;

$$\bar{J}=\nabla\times\bar{T} \tag{4}$$

From Maxwell's equation we have;

$$\nabla\times\bar{H}=\bar{J}=\nabla\times\bar{T} \tag{5}$$

Then;

$$\nabla\times\left(\bar{H}-\bar{T}\right)=0 \tag{6}$$

Since the vector $(H-T)$ can be expressed as the gradient of a scalar, i.e.,

$$\bar{H}=\bar{T}-\nabla\Omega \tag{7}$$

where, Ω is a magnetic scalar potential.

And, Since

$$\nabla\times\bar{E}=-\frac{\partial\bar{B}}{\partial t} \tag{8}$$

Then;

$$\begin{aligned}\nabla\times\bar{E}=\nabla\times\left[\left(\frac{1}{\sigma}\right)\nabla\times\bar{T}\right]&=-\frac{\partial\bar{B}}{\partial t}=-\mu_0\mu_r\left(\frac{\partial}{\partial t}\right)(\bar{T}-\nabla\Omega)\\&=-\mu_0\mu_r\left(\frac{\partial\bar{T}}{\partial t}\right)-\nabla\left(\frac{\partial\Omega}{\partial t}\right)\end{aligned} \tag{9}$$

which finally reduces to the following two scalar equations

$$\nabla^2 \bar{T} - \mu\sigma \left(\frac{\partial \bar{T}}{\partial t} \right) = -\mu\sigma \nabla \left(\frac{\partial \Omega}{\partial t} \right) \tag{10}$$

And

$$\nabla^2 \Omega = 0 \tag{11}$$

when a three dimensional magnetic field problem is solved by A and V, the need to solve for all the three components of A arises, whereas using the $T - \Omega$ method, T can be simplified to produce a solution with only two components of T. Also, in this analysis, the usual assumptions such as the magnetic field outside of an air box in which the motor is placed considered to be zero. In order to represent the motor operation and determine the various parameters at different rotor positions, the analysis includes a 360 degree rotation of the rotor to analyze SRM behavior at the different rotor positions.

3.1. Workbench of the Simulation

The motor configuration and specifications used in this study are shown in Fig. 2 and Table 1, respectively. The motor phases are clearly marked for later use in Fig. 2.

Table 1. 6/4 SR motor dimensions.

Parameter	Value
Stator core outer diameter	72 mm
Rotor core outer diameter	40.5 mm
Stack length	35 mm
Length of air gap	0.25 mm
Shaft diameter	10 mm
Rotor pole arc	32°
Stator pole arc	28°
Number of turns	120

The stator and rotor cores are made up of non-oriented silicon steel laminations and also, each phase winding consists of 120 turns with a current magnitude of 2.5 A. Due to precise comparison between healthy and faulty mode with FE analysis, the mesh densities and other conditions are considered to be exactly the same for both cases. The FE model with mesh densities used in the simulation is shown in Fig. 3.

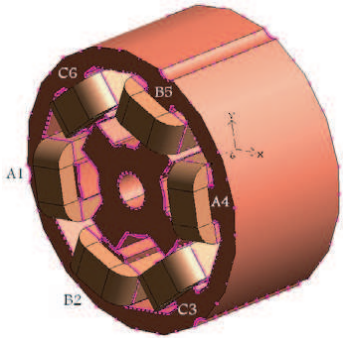

Figure 2. 6/4 SR Motor 3D-FEM model assembly.

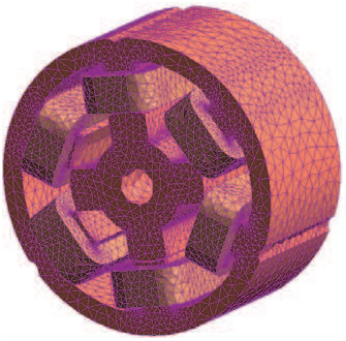

Figure 3. 3D-finite element mesh density for the SRM.

4. NUMERICAL RESULTS AND ANALYSIS

As stated, the proposed 3D-finite element method is employed to evaluate the performance of the motor under angular misalignment fault. In this regards the effect of this type of fault upon main profiles and magnetostatic characteristic of the motor are obtained and analyzed for flux density, flux linkage, inductance and mutual inductance.

4.1. Impacts of Angular Misalignment on Magnetic Flux Density

Regarding to the following equation, variation of magnetic flux density (B) in airgap can be considered proportional to the variation of current flow;

$$\oint Bdl = \mu I \tag{12}$$

Therefore, the evaluation of motor operation requires accurate knowledge of the flux distribution inside the SR motor for different rotor positions in various levels of fault.

Magnetic flux density arrows of the rotor in healthy mode and the motor with 50% angular misalignment utilizing FE analysis are shown in Fig. 4. In these figures rotor and stator are shown separately for better illustration, also the fault occurred in phase B that its stator pole overlaps fully with rotor pole.

The angular misplacement has happened in line with y axis as explained in Fig. 1. Moreover; the airgap non-uniformity is different through the z axis. Consequently the distribution of the airgap in front of the two poles of the same rotor phase as well as the magnetic

flux density is asymmetrical as depicted in Fig. 4(b), while these flux densities are symmetrical in healthy motor (Fig. 4(a)).

Magnetic flux density shadows of the stator in healthy mode and motor with 50% angular misalignment utilizing FE analysis are shown in Fig. 5.

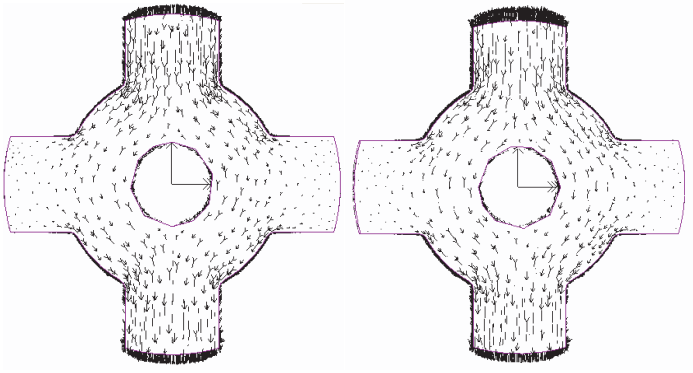

(a) (b)

Figure 4. Magnetic flux density arrows of the rotor in (a) healthy motor (b) motor with 50% angular misalignment.

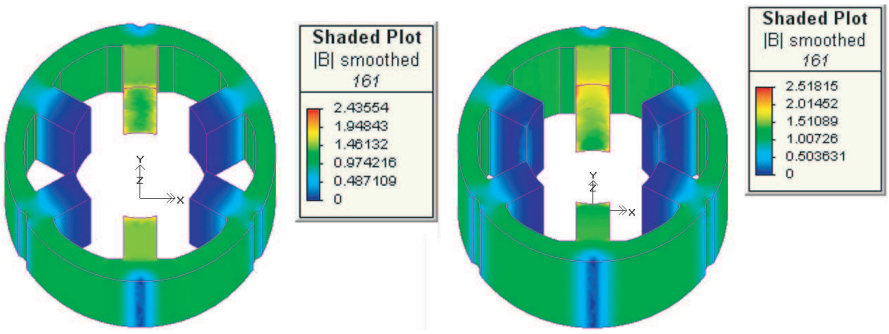

(a) (b)

Figure 5. Magnetic flux density shadow of the stator in (a) healthy motor (b) motor with 50% angular misalignment.

The behavior of magnetic flux density in the rotor is repeated in stator poles. As presented in Fig. 5 the flux density distribution has been uniform along the stator poles in the excited phase for healthy mode but is in an unbalanced mode with occurrence of angular misalignment. In respect to essence of this type of fault other phases have a similar behavior when they are excited.

As presented in Fig. 5 when the rotor and stator poles have

overlapped in faulty phase, the air gap length in front of the stator pole of phase B (B-2) along z axis is varied and the amplitude of magnetic flux density goes up to 2.51 Tesla in the direction of the shortest air gap. Whereas this profile on the other side of this pole is 1.5 Tesla, in which magnetic flux density is changed 67% under occurrence of 50% misalignment fault, along with z axis.

The airgap length variation in the front of faulty phase leads to variation of its related magnetic reluctance which causes a variation in the flux density. Regarding to the Maxwell stress tensors the Unbalanced Magnetic Pull (UMP) is produced along the poles and led to more noise and vibration in the SR motor.

4.2. Impacts of Angular Misalinment on Flux Linkage and Inductance

In SR motor operation, it is very important to establish the flux linkage (λ) waveforms in each part of the core. Flux linkage in SR motor is depended on phase current which is function of the motor speed and load. On the other hand, variation of inductance (L) versus rotor position is high-quality profile of SR motor control and analysis. The effective inductance is defined as the ratio of each phase flux linkages to the exciting current ($\lambda(\theta)/I$). Flux linkage of the motor phases including A, B and C versus rotor position for healthy motor is obtained and presented in Fig. 6. As depicted, the shape of the flux linkage waveforms are almost uniform in all phases, therefore, the inductance magnitudes have the same value.

Figure 7 shows the motor flux linkage, and the variation of rotor position in healthy motor as well as the motor with a range of angular misalignments in 360° rotation of the rotor. In this figure the fault has been occurred in phase C. The occurrence of angular misalignment has led to variety of flux values for this phase. As shown in Fig. 7, with an increase in the angular misalignment, flux linkage of coil 3 belonging to the phase C as well as its inductance has increased. For example, the flux linkage of this coil in the first excitation increased by nearly 10% in peak value with occurrence of 50% fault. The rotor position detection in controlling SRM depends on inductance changes due to the nature of reluctance torque development. Hence, sensing the abnormal deviations of the inductances due to angular misalignment fault can produce errors in the triggering of the power switches in the drive circuitry.

These flux variations and their amplitudes are depended on the rotor position and speed, in which with any changes in these profiles, the effects of fault will be show different results. Thus, mutual

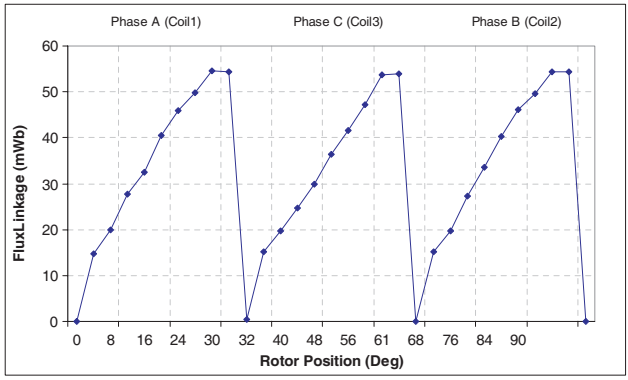

Figure 6. Flux linkage in all phases of the SRM.

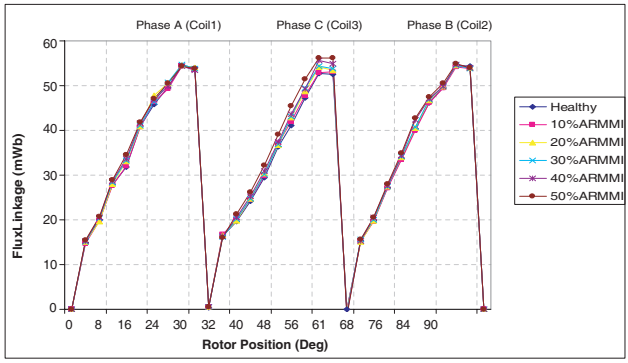

Figure 7. Flux linkage in all phases of the SRM under various degree of angular misalignment fault.

inductance evaluation can be a helpful tool for a clear analysis and diagnosis for this type of fault.

4.3. Impacts of Angular Misalinment on Mutual Inductance

The driven equipments may generate a force across the excited poles which attempts to either push or pull the rotor from its magnetic center [35]. Thus, under fault conditions, the changes of the inductance as well as mutual inductance values are required to be considered for maintaining the desired level of operation.

The mutual inductance is the ratio of induced magnetic flux linkage to the current; therefore, the mutual inductance is directly proportional to the induced flux linkage.

When the fault is occurred with various levels of angular

misalignment and phase B is excited, the mutual inductance values in coils 1, 4 belonging to phases A are obtained and shown in Fig. 8, Fig. 9 respectively. In these figures a third order polynomials have been fitted through the data points for different levels of fault for better interpretations of the results.

As seen from Fig. 8 and Fig. 9, the slopes of mutual inductance increase when the fault levels go up, and also the magnitudes of mutual inductance for each angular misalignment level increase when the phase B is excited. Also as shown in theses figures, the amplitude of the mutual inductance in A-1 for 50%, 40%, 30%, 20% and 10% fault is about 1.85, 1.28, 1.07, 0.57 and 0.28 times higher than amplitude of mutual inductance in healthy motor, for maximum variation. The mutual inductance in A-4 shows similar behavior but different amplitudes.

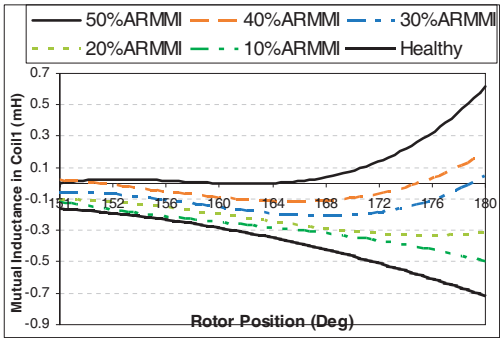

Figure 8. Mutual inductance in coil 1 from phases A when B excited, in healthy and angular misaligned SR motor.

Considering the slope of linear approximation for the mutual inductance in phase A one can gains acknowledge about variation of maximum and minimum mutual inductances, which play important role in produced torque. It is observed that the slope of mutual inductance in Fig. 9 for A-4 has 5, 9, 17, 20 and 33 times higher value than slope of mutual inductance in healthy motor, when the phase B excited. The slope of mutual inductance in A-1 shows similar behavior to A-4 but with different values. On the other hand, this type of fault increases the difference between maximum and minimum mutual inductance values in coils 1, 4 from phase A.

Figures 10 and 11 show the calculated mutual inductances in coil 1, 4 belonging to phase A while phase C is excited and different levels of angular misalignment fault are applied. Also third order polynomial approximation is utilized for various levels of fault to achieve more accuracy.

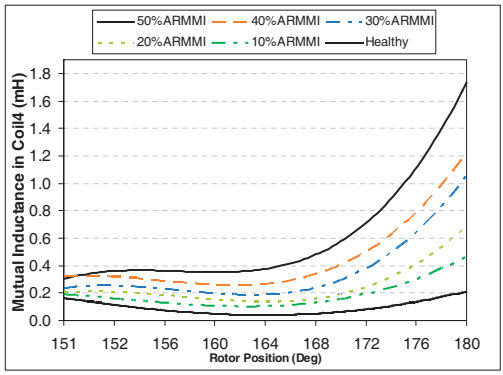

Figure 9. Mutual inductance in coil 4 from phases A when B excited, in healthy and angular misaligned SR motor.

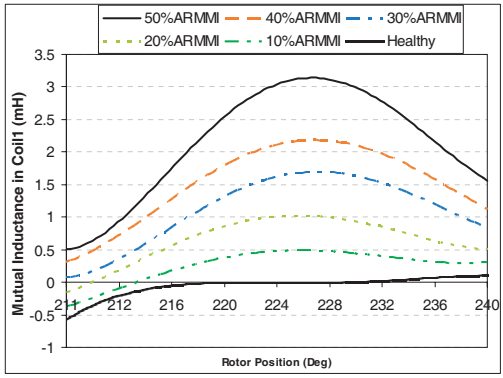

Figure 10. Mutual inductance in coil 1 from phases A when C excited, in healthy and angular misaligned SR motor.

As expected, the mutual inductances in phase A, when phase C is excited, have different shapes in comparison with their values when phase B is excited. These variations are depended on the rotor speed and position, while these shapes are similar for both excitations in healthy motor. On the other hand, it is to be noted here that mutual inductance varies sinusoidal with rotor position in the presence of this type of fault. Therefore, it leads to asymmetrically distribution of electromagnetic behavior of the motor which produces noise and vibrations. The variation of mutual inductance waveform in A-1 is low in healthy condition.

Since the produced torque and induced voltage in SR machines

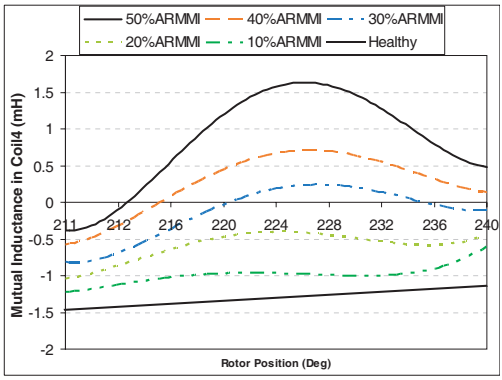

Figure 11. Mutual inductance in coil 4 from phases A when C excited, in healthy and angular misaligned SR motor.

are directly proportional to the variation of inductance with respect to the rotor position, then the torque and voltage production profiles in motoring and generating modes of operation will vary accordingly. The following formulas for the SR machine in the linear mode of operation will prove the above statement.

$$T = \frac{1}{2} i^2 \frac{dL}{d\theta} \tag{13}$$

$$e_{ind} = \omega \frac{d\lambda}{d\theta} \tag{14}$$

As a result; the amplitude and slope of mutual inductance in both coils of inactive phase can be a good indicator for diagnosing this type of fault, that the level of angular misalignment fault can be detected.

Consequently, when considering the mutual inductance variation of the inactive phase in two consecutive excitations, the direction of deviation of the rotor center (O'_R in Fig. 1) can be detected.

5. CONCLUSION

In this paper, the magnetostatic analysis of the angular misalignment fault in a switched reluctance motor is performed. For this purpose the angular misalignment was modeled and analyzed using 3D-FEM by considering the end effects and axial fringing fields for implementation of a reliable model. Afterwards, the main results are compared with those obtained from healthy motor. The flux density distribution has been non-uniform along the stator poles in excited phase in faulty mode. The magnetic flux density along the stator poles in excited

phase is changed 67% under 50% angular misalignment fault. Also, an increase in the level of fault causes the flux linkage of excited phase as well as its inductance will increase. For example, the flux linkage of phase C in first excitation increased almost by 10% in peak value with occurrence of 50% fault. Moreover, it is shown that the slope and amplitude of mutual inductances of inactive phases are increased when degree of fault goes up. Also, when phase B excited the amplitude of the mutual inductance in one coil and slope of other coil of phase A for 50% fault is about 1.85 and 33 times higher in healthy motor, for maximum variation, respectively. These variations are repeated for phase A when the phase C excited, however with different shapes. Accordingly, the amplitude and slope of mutual inductance in both coils of inactive phase in two consecutive excitations are introduced as a good candidate for diagnosing this type of fault, level of angular misalignment as well as direction of occurrence.

ACKNOWLEDGMENT

The author would like to thank Prof. Afjei for his reviewing and editing of this paper. This work was supported by Young Researchers Club of I.A.U., South Tehran Branch.

REFERENCES

1. Torkaman, H. and E. Afjei, "Hybrid method of obtaining degrees of freedom for radial airgap length in SRM under normal and faulty conditions based on magnetiostatic model," *Progress In Electromagnetics Research*, PIER 100, 37–54, 2010.
2. Torkaman, H. and E. Afjei, "Magnetio static field analysis regarding the effects of dynamic eccentricity in switched reluctance motor," *Progress In Electromagnetics Research M*, Vol. 8, 163–180, 2009.
3. Afjei, E. and H. Torkaman, "The novel two phase field-assisted hybrid SRG: Magnetio static field analysis, simulation, and experimental confirmation," *Progress In Electromagnetics Research B*, Vol. 18, 25–42, 2009.
4. Husain, I., A. Radun, and J. Nairus, "Fault analysis and excitation requirements for switched reluctance generators," *IEEE Power Engineering Review*, Vol. 22, No. 2, 57–58, 2002.
5. Miller, T. J. E., "Faults and unbalanced forces in the switched reluctance machine," *IEEE Transaction on Industry Applications*, Vol. 31, 319–328, 1995.
6. Babic, S. I., F. Sirois, and C. Akyel, "Validity check of mutual inductance formulas for circular filaments with lateral and angular

misalignments," *Progress In Electromagnetics Research M*, Vol. 8, 15–26, 2009.

7. Dorrell, D. G., "Sources and characteristics of unbalanced magnetic pull in 3-phase cage induction motors with axial-varying rotor eccentricity," *IEEE Energy Conversion Congress and Exposition, ECCE*, San Jose, California, 2009.
8. Lundin, U. and A. Wolfbrandt, "Method for modeling time-dependent nonuniform rotor/stator configurations in electrical machines," *IEEE Transactions on Magnetics*, Vol. 45, No. 7, 2976–2980, 2009.
9. Heidrich, P. and R. Hanitsch, "Simulation of a completely controlled switched reluctance drive with eccentric rotor using a time-stepping technique realised outside numerical field calculation programs," *IEEE Transactions on Magnetics*, Vol. 32, No. 3, 1565–1568, 1996.
10. Li, J., D. Choi, and Y. Cho, "Analysis of rotor eccentricity in switched reluctance motor with parallel winding using FEM," *IEEE Transactions on Magnetics*, Vol. 45, No. 6, 2851–2854, 2009.
11. Zhu, Z. Q., et al., "Significance of vibration modes in noise and vibration generation of switched reluctance motors," *Sixth Inter. Conf. on Electrical Machines and Systems, ICEMS*, 2003.
12. Chindurza, I., D. G. Dorrell, and C. Cossar, "Non-invasive fault diagnosis for switched-reluctance machines with incorrect winding turns, inter-turn winding faults and eccentric rotors," *Fifth International Conference on Power Electronics and Drive Systems, PEDS*, 2003.
13. Chindurza, I., D. G. Dorrell, and C. Cossar, "Vibration analysis of a switched-reluctance machine with eccentric rotor," *Second International Conference on Power Electronics, Machines and Drives, PEMD*, 2004.
14. Briso-Montiano, J. R., R. Karrelmeyer, and E. Dilger, "Simulation of faults by means of finite element analysis in a switched reluctance motor," *Multiphysics Conference*, Comsol, Inc., Frankfurt, USA, 2005.
15. Dorrell, D. G., I. Chindurza, and C. Cossar, "Effects of rotor eccentricity on torque in switched reluctance machines," *IEEE Transactions on Magnetics*, Vol. 41, No. 10, 3961–3963, 2005.
16. Dorrell, D. G. and C. Cossar, "A vibration-based condition monitoring system for switched reluctance machine rotor eccentricity detection," *IEEE Transactions on Magnetics*, Vol. 44, No. 9, 2204–2214, 2008.

17. Garrigan, N. R., et al., "Radial force characteristics of a switched reluctance machine," *IEEE Industry Applications Conference, Thirty-Fourth IAS Annual Meeting*, 1999.
18. Jinghua, J., et al., "Calculation and remedial strategy of radial force of switched reluctance motors with eccentricity," *International Conference on Electrical Machines and Systems, ICEMS*, 2008.
19. Torkaman, H. and E. Afjei, "Comprehensive study of 2-D and 3-D finite element analysis of a switched reluctance motor," *Journal of Applied Sciences*, Vol. 8, No. 15, 2758–2763, 2008.
20. Afjei, E., A. Seyadatan, and H. Torkaman, "A new two phase bidirectional hybrid switched reluctance motor/field-assisted generator," *Journal of Applied Sciences*, Vol. 9, No. 4, 765–770, 2009.
21. Toulabi, M. S., H. Torkaman, and E. Afjei, "Magnetostatic analysis of a novel switched reluctance generator," *IEEE 1st Power Electronic and Drive Systems and Technologies Conference, PEDSTC*, Tehran, Iran, 2010.
22. Torkaman, H. and E. Afjei, "Comprehensive magnetic field-based study on effects of static rotor eccentricity in switched reluctance motor parameters utilizing three-dimensional finite element," *Electromagnetics*, Vol. 29, No. 5, 421–433, 2009.
23. Ravaud, R. and G. Lemarquand, "Comparison of the coulombian and amperian current models for calculating the magnetic field produced by radially magnetized arc-shaped permanent magnets," *Progress In Electromagnetics Research*, PIER 95, 309–327, 2009.
24. Panda, D. K. K., A. Chakraborty, and S. R. Choudhury, "Analysis of co-channel interference at waveguide joints using multiple cavity modeling technique," *Progress In Electromagnetics Research Letters*, Vol. 4, 91–98, 2008.
25. Lu, H. H., C. H. Lee, P. W. Ko, C. H. Kuo, C. C. Liu, H. B. Wu, and J. S. Shin, "Direct-detection bidirectional radio-on-DWDM transport systems," *Journal of Electromagnetic Waves and Applications*, Vol. 23, No. 7, 875–884, 2009.
26. Zhang, Y. J. and E. P. Li, "Scattering of three-dimensional chiral objects above a perfect conducting plane by hybrid finite element method," *Journal of Electromagnetic Waves and Applications*, Vol. 19, No. 11, 1535–1546, 2005.
27. Pingenot, J., R. N. Rieben, D. A. White, and D. G. Dudley, "Full wave analysis of RF signal attenuation in a lossy rough surface cave using a high order time domain vector finite element method," *Journal of Electromagnetic Waves and Applications*,

Vol. 20, No. 12, 1695–1705, 2006.

28. Ozgun, O. and M. Kuzuoglu, "Finite element analysis of electromagnetic scattering problems via iterative leap-field domain decomposition method," *Journal of Electromagnetic Waves and Applications*, Vol. 22, No. 2–3, 251–266, 2008.
29. Zhang, Y., X. Wei, and E. Li, "Electromagnetic scattering from three-dimensional bianisotropic objects using hybrid finite element-boundary integral method," *Journal of Electromagnetic Waves and Applications*, Vol. 18, No. 11, 1549–1563, 2004.
30. Wang, Q. and X.-W. Shi, "An improved algorithm for matrix bandwidth and profile reduction in finite element analysis," *Progress In Electromagnetics Research Letters*, Vol. 9, 29–38, 2009.
31. Tai, C.-C. and Y.-L. Pan, "Finite element method simulation of photoinductive imaging for cracks," *Progress In Electromagnetics Research Letters*, Vol. 2, 53–61, 2008.
32. San-Blas, A. A., F. Mira, J. Gil, V. E. Boria, and B. Gimeno Martinez, "Efficient analysis and design of compensated turnstile junctions using advanced modal techniques," *Progress In Electromagnetics Research Letters*, Vol. 12, 21–30, 2009.
33. Ravaud, R., G. Lemarquand, V. Lemarquand, and C. Depollier, "The three exact components of the magnetic field created by a radially magnetized tile permanent magnet," *Progress In Electromagnetics Research*, PIER 88, 307–319, 2008.
34. Magnet CAD package, *User Manual*, Infolytica Corporation Ltd., Montreal, Canada, 2007.
35. Ravaud, R., G. Lemarquand, V. Lemarquand, S. I. Babic, and C. Akyel, "Mutual inductance and force exerted between thick coils," *Progress In Electromagnetics Research*, PIER 102, 367–380, 2010.
36. Steinbauer, M., R. Kubasek, and K. Bartusek, "Numerical method of simulation of material influences in MR tomography," *Progress In Electromagnetics Research Letters*, Vol. 1, 205–210, 2008.
37. Suyama, T., Y. Okuno, A. Matsushima, and M. Ohtsu, "A numerical analysis of stop band characteristics by multilayered dielectric gratings with sinusoidal profile," *Progress In Electromagnetics Research B*, Vol. 2, 83–102, 2008.
38. Urbani, F., "Numerical analysis of periodic planar structures on uniaxial substrates for miniaturization purposes," *Progress In Electromagnetics Research Letters*, Vol. 5, 131–136, 2008.